Open Access

Journal of Energy and Power Technology

LIDSEN Publishing Inc.

Original Research

Stability Improvement of Multimachine System Using Back-To-Back Converters

Minyang Wang [1], Daming Zhang [1, *], Liang Yuan [2]

1. School of Electrical Engineering and Telecommunication, University of New South Wales, Sydney, Australia; E-Mails: z5285835@ad.unsw.edu.au; daming.zhang@unsw.edu.au
2. School of Automation, Central South University, Changsha, China; E-Mail: liang.yuan@csu.edu.cn

* **Correspondence:** Daming Zhang; E-Mail: daming.zhang@unsw.edu.au

Academic Editor: Rodolfo Dufo-López

Special Issue: Design and Operation of Microgrids

Journal of Energy and Power Technology
2024, volume 6, issue 4
doi:10.21926/jept.2404021

Received: July 15, 2024
Accepted: November 12, 2024
Published: November 15, 2024

Abstract

As the penetration level of inverter-based generators continues to increase, it becomes crucial to reduce power oscillations between inverters and synchronous generators (SG) to improve system stability. This paper uses a multimachine system as the research platform and proposes a grid separation method employing a multi-terminal back-to-back converter. The converter is designed to be placed at the point of common coupling (PCC) in the original multimachine system and can divide the original grid into multiple microgrid regions while retaining the ability to transmit power between different regions. Each microgrid or region contains a self-regulated power source such as grid-forming (GFM) inverter or synchronous generator, which controls key power characteristics such as frequency and voltage within its region. The back-to-back converter facilitates power transmission between different regions. The AC-DC-AC conversion process ensures isolation and simplification of control over each microgrid's power characteristics. The performance of inverters with different control strategies in each microgrid has been investigated, and the characteristics of various inverters are compared and demonstrated. Additionally, it was found that the battery storage

requirements in each inverter-based microgrid are reduced using this method. The results are verified through MATLAB/SIMULINK simulations.

Keywords
Microgrid; power oscillation; grid-forming inverter; grid separation; back-to-back converter

1. Introduction

With the advancement of technology and the development of industry, the overall capacity of sustainable energy generation has significantly increased over the past decades. Figure 1 demonstrates the growth of global wide electricity capacity from 2011 to 2023 which includes significant increase of the penetration of inverter-based generators [1, 2]. Eco-friendly energy sources such as PV panels and wind turbines depend on these power electronic devices to connect to the existing power grid. As a result, the proportion of kinetic energy stored in the traditional synchronous generators' physical rotors has decreased, leading to a decline in grid inertia and an increase in equivalent grid impedance [3, 4]. Consequently, the power grid's ability to withstand disturbances has been dwindling, bringing potential instability concerns to the power grid.

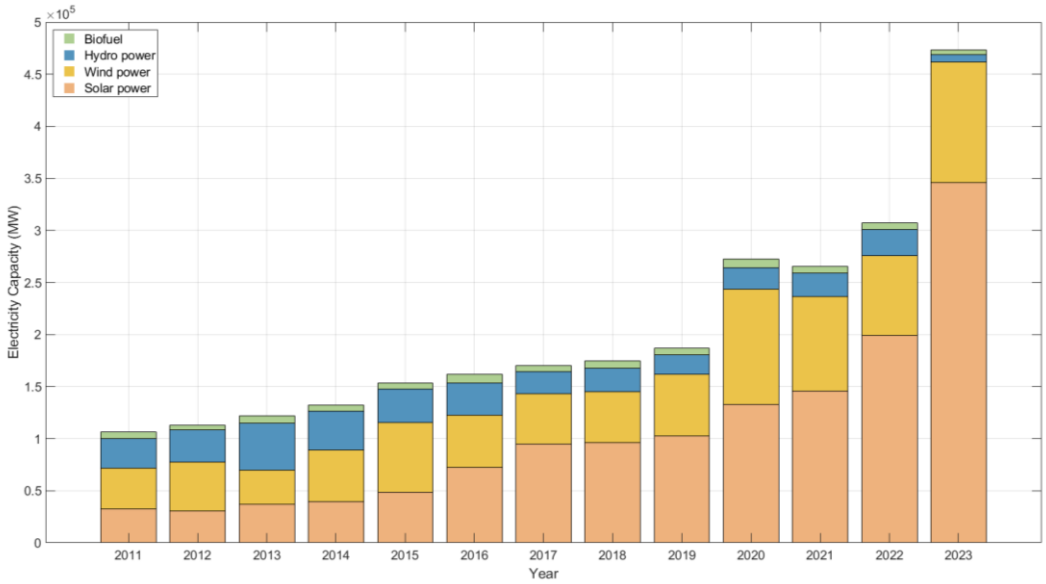

Figure 1 Global wide electricity capacity of sustainable energy from 2011 to 2023.

One mainstream grid-connected inverter is the grid-following (GFL) inverter, which typically relies on a phase-locked loop (PLL) to synchronize with the existing power grid [5]. Paper [6] has demonstrated that for accurate synchronization and stable operation, the equivalent impedance between the PCC and the power grid must be low, making the GFL inverter better suited for operation in strong grid conditions. Paper [7] has demonstrated that the traditional GFL inverter offers advantages such as fast demand response and ease of achieving stable operation when multiple GFL inverters are connected in parallel. However, a key disadvantage is that GFL inverters require a strong power grid for connection, but the grid strength continues to decrease as the

number of GFL inverters increases. Thus, a trade-off is necessitated between system stability and the number of GFL inverters connected in parallel.

To achieve better inertia and ensure stable operation in weak grids when grid impedance is large, the frequency and voltage of the power grid need to be supported. Thus, the static synchronous compensator (STATCOM) [8, 9] and grid-forming (GFM) inverters [10-12] are developed to improve power quality in distributed energy resources. Paper [8] has shown that the STATCOM is an external equipment that is parallel connected at the PCC point. It can detect voltage deviations, autonomously inject reactive power to maintain the AC bus voltage within operational limits, eliminate power fluctuations, and improve system stability in grids with moderate penetration of inverter-based generators. Paper [10] has shown that the GFM inverter is the equipment that replicates the voltage and frequency regulation behavior of a synchronous generator. It can adjust its control parameters to meet system operation requirements, ensures a fast response to restore system stability, and has the advantages such as automatic grid support and the ability to operate in both grid-connected and island modes. However, new challenge has emerged with GFM inverters, paper [11] and paper [12] both pointed out that when multiple GFM inverters are connected in parallel or to a strong power grid, power oscillations can occur between the GFM inverters or with other power sources. This is the issue that this paper aims to address.

The comparison of the dynamic performance between different inverters under the single-machine-infinite-bus (SMIB) system has been well investigated. The finding is that all types of GFM inverters can respond to frequency and voltage deviations and improve system inertia [10]. And the GFM inverter using virtual synchronizing generator (VSG) control has better fault ride-through (FRT) capability [13] and a wider operation range [14], which makes it a better foundational configuration for the research. However, the actual power network with one PCC point usually containing multiple inverters and loads is more complicated than an SMIB system, so stability research for a multimachine system is required. Considering that GFL inverters and GFM inverters have different ranges of adaptation to grid strength with minimal overlap, when multiple GFL inverters and GFM inverters are connected in parallel at the same PCC point, the grid strength that can ensure stable operation for all inverters will also be relatively limited, which indicates that such system has relatively poor resilience to disturbances. Without additional control strategies, large disturbances could affect the synchronization between inverters and the power grid, cause power oscillations, and ultimately compromise system stability.

To address this issue, this paper proposes a grid separation method using a multi-terminal back-to-back converter. The main contributions are summarized as: 1) separating large power grids into multiple small microgrids using the proposed method; 2) reducing power oscillations while maintaining power-sharing capabilities; 3) investigating the dynamic performance of the modified system under various conditions.

The remaining part of this paper is outlined as follows: Section II presents the circuit structure of the multimachine system, the control strategy of different inverters, and the configuration of the proposed back-to-back converter. Section III conducts simulations to compare the dynamic performance of the multimachine system with and without the proposed back-to-back converter under different conditions. Section IV discusses the findings and system stability based on the simulation results. Section V concludes the paper.

2. Circuit Structure and Control Configurations

2.1 Circuit Structure

2.1.1 Original Multimachine System

In the first study of this paper, two inverters, one STATCOM, one synchronous generator, and three constant loads are included in a multimachine system, whose circuit structure is shown in Figure 2. The output terminal of each power source is connected to one local constant load (20 kW) and one local switchable load (10 kW). The line impedances between inverters and the PCC point are considered due to long cables over the distance. The multimachine system is set to operate at 50 Hz, 415 V and the overall loads are 60 kW with each of three constant loads Z_{load1}, Z_{load2} and Z_{load3} being 20 kW. Each of three switchable loads Z_{Dstb1}, Z_{Dstb2} and Z_{Dstb3} in Figure 2 is 10 kW and used as disturbance. The grid strength is characterized by the short circuit ratio (SCR).

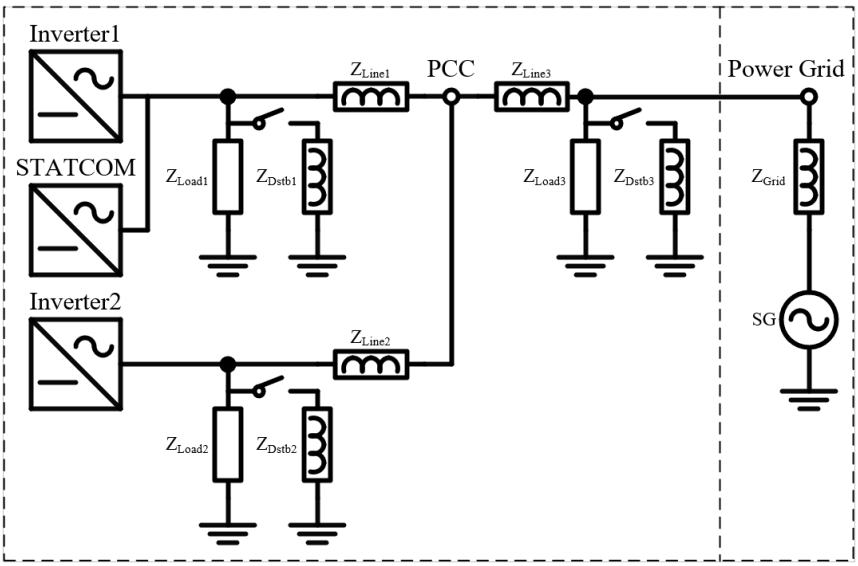

Figure 2 Circuit structure of the original multimachine system.

The equations to calculate the SCR of this multimachine system are demonstrated below:

$$SCR = \frac{1}{P_{ratedall}}\left(P_{rated1}k_{SC1} + P_{rated2}k_{SC2} + \frac{{V_{SG}}^2}{|Z_{SC3}|}\right) \quad (1)$$

$$Z_{SC3} = \frac{Z_{Line3}Z_{Load3}}{Z_{Line3} + Z_{Load3}} + Z_{Grid} \quad (2)$$

where $P_{ratedall}$ represents the overall rated power of the multimachine system, P_{rated1} represents the rated power of inverter 1, k_{SC1} represents the short circuit capacity ratio of inverter 1, P_{rated2} represents the rated power of inverter 2, k_{SC2} represents the short circuit capacity ratio of inverter 2, V_{SG} represents the voltage value of the synchronous generator, and Z_{SC3} represents the equivalent impedance between the synchronous generator and the PCC point. In this paper, only the grid impedance, line impedance, and constant load are used to calculate the short circuit power, the

impedance of disturbance is not considered, and the impedance of local loads, local disturbances, and lines are the same for inverter 1, inverter 2 and synchronous generator.

2.1.2 Modified System

The proposed grid separation method places a three-terminal back-to-back converter at the original PCC point to divide the multimachine system into three separate microgrids, each with its own grid impedance while retaining the ability to share power through the back-to-back converter. Each terminal of the back-to-back converter contains six MOSFETs and one LC filter, and there is a large capacitor at the DC side of the converter. The proposed back-to-back converter is designed to operate under grid-following mode and will only share active power between different microgrid regions. The reactive power in each microgrid is provided by the grid-forming inverter or synchronous generator only, with no interaction between other microgrids. The circuit structure of the modified system with the proposed back-to-back converter is shown in Figure 3.

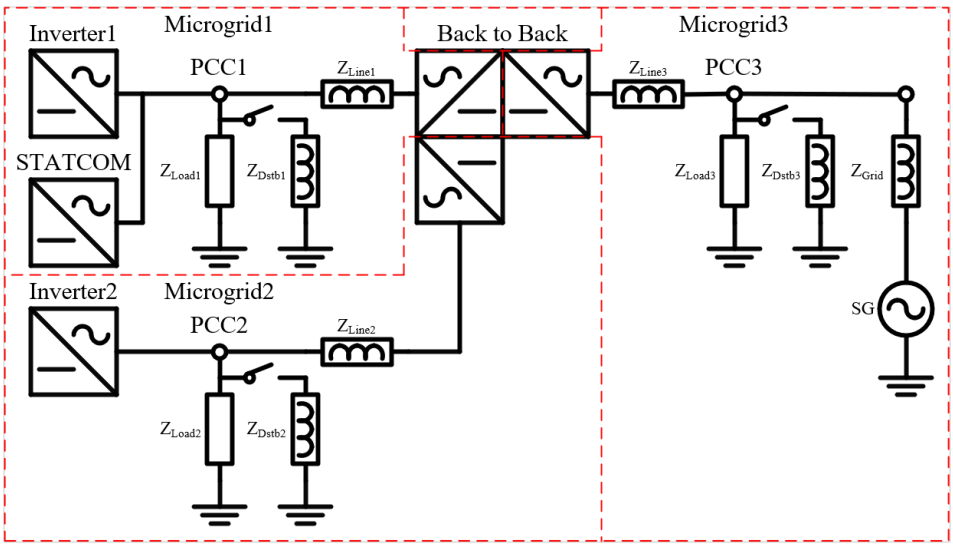

Figure 3 Circuit structure of the modified system with a back-to-back converter.

The equations to calculate the SCRs of each microgrid are demonstrated below:

$$SCR1 = \frac{P_{rated1}k_{SC1} + P_{BTB1}}{P_{rated1}} \tag{3}$$

$$SCR2 = \frac{P_{rated2}k_{SC2} + P_{BTB2}}{P_{rated2}} \tag{4}$$

$$SCR3 = \frac{{V_{SG}}^2}{P_{rated3}|Z_{Grid}|} \tag{5}$$

where P_{BTB1} represents the power transmitted from the back-to-back converter to microgrid 1, P_{BTB2} represents the power transmitted from the back-to-back converter to microgrid 2, P_{rated3} represents the rated power of the synchronous generator, Z_{Grid} represents the grid impedance between the synchronous generator and the PCC point in microgrid 3.

2.2 Control Strategy

2.2.1 Control Strategy of Inverter 1

Inverter 1 is a grid-forming inverter that uses constant frequency control. Different from other typical grid-forming inverters that use the power synchronization method, this control method employs a PLL to synchronize with the power grid in grid-connected mode and an internally generated virtual theta angle in island mode [15]. Additionally, it requires a STATCOM at its output terminal to ensure voltage stability, which performs as an autonomous reactive power compensator. Different from droop or VSG control, this constant frequency control produces real power reference based on its terminal voltage deviation from the rated voltage or a pre-set value slightly higher than the rated voltage [16]. In some applications, its real power output reference can be set to a constant value. The active power reference generation for the grid-following generator could be the same as that for the grid-forming generator, i.e. it is produced based on its terminal voltage deviation from the targeted one. The system demanded reactive power is handled by the STATCOM, therefore, the reactive power output reference for the grid-forming inverter can be set as 0.

For this case, inverter 1 serves as the grid-forming generator while the one connected with back-to-back converter serves as a grid-following generator with a pre-planned power import from the microgrid with synchronous generator. The control loops of the inverter 1 are demonstrated in Figure 4(a) and the control loops of the grid-following inverter at the microgrid 1's side of the back-to-back converter are demonstrated in Figure 4(b).

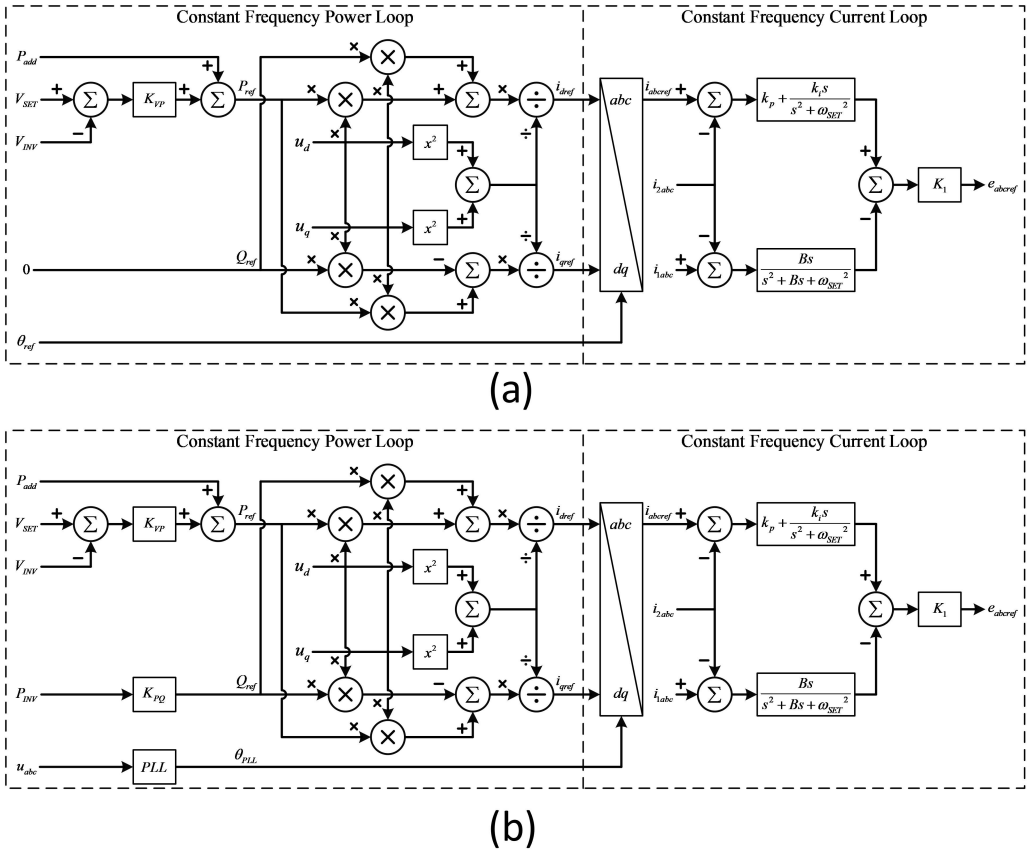

Figure 4 (a) Constant frequency control loops: grid-forming mode. (b) Constant frequency control loops: grid-following mode.

Equations (6) demonstrates the power loop of constant frequency control under grid-forming mode:

$$\begin{bmatrix} P_{ref} \\ Q_{ref} \\ \theta_{ref} \end{bmatrix} = \begin{bmatrix} K_{VP}(V_{SET} - V_{INV}) + P_{add} \\ 0 \\ \theta_{virtual} \end{bmatrix} \tag{6}$$

where K_{VP} represents the droop coefficient between voltage and active power, V_{SET} represents the rated operating voltage or other pre-set value slightly above the rated one, V_{INV} represents the measured voltage of the inverter, P_{add} represents the compensated active power, P_{ref} represents the reference active power, Q_{ref} is set as 0, and ϑ_{ref} is internally generated through a virtual three phase signal.

Equation (7) and (8) demonstrate the current loop using PR control:

$$\begin{bmatrix} i_{dref} \\ i_{qref} \end{bmatrix} = \begin{bmatrix} \frac{u_d}{{u_d}^2 + {u_q}^2} & \frac{u_q}{{u_d}^2 + {u_q}^2} \\ \frac{u_q}{{u_d}^2 + {u_q}^2} & \frac{-u_d}{{u_d}^2 + {u_q}^2} \end{bmatrix} \begin{bmatrix} P_{ref} \\ Q_{ref} \end{bmatrix} \tag{7}$$

$$\begin{bmatrix} e_{aref} \\ e_{bref} \\ e_{cref} \end{bmatrix} = K_1 \left(\left(k_p + \frac{k_i s}{s^2 + {\omega_{SET}}^2} \right) \left(\begin{bmatrix} i_{aref} \\ i_{bref} \\ i_{cref} \end{bmatrix} - \begin{bmatrix} i_{2a} \\ i_{2b} \\ i_{2c} \end{bmatrix} \right) - \frac{Bs}{s^2 + Bs + {\omega_{SET}}^2} \left(\begin{bmatrix} i_{1a} \\ i_{1b} \\ i_{1c} \end{bmatrix} - \begin{bmatrix} i_{2a} \\ i_{2b} \\ i_{2c} \end{bmatrix} \right) \right) \tag{8}$$

where u_d and u_q represent the real-time dq-axis voltage, i_{dref} and i_{qref} represent the inverter dq-axis internal reference current, K_1 is the parameter of a P controller, k_p and k_i are the parameters of a PR controller, B is the parameter of a bandpass filter, ω_{SET} represents the rated angular frequency of the system, i_{2abc} represent the measured grid-side current, i_{1abc} represent the measured inverter-side current, e_{abcref} represent the inverter internal reference voltage. One important thing is that the stationary frame reference current i_{abcref} are calculated through inverse Park transformation of the rotating frame reference current i_{dqref}. The angle to conduct inverse Park transformation is internally generated through a virtual three phase signal when operating under the grid-forming mode, or calculated through a PLL tracking the real-time phase angle at the connecting point when operating under grid-following mode in grid-connected conditions.

Equation (9) demonstrates the power loop of constant frequency control under grid-following mode:

$$\begin{bmatrix} P_{ref} \\ Q_{ref} \\ \theta_{PLL} \end{bmatrix} = \begin{bmatrix} K_{VP}(V_{SET} - V_{INV}) + P_{add} \\ K_{PQ} P_{INV} \\ G_{PLL} u_{abc} \end{bmatrix} \tag{9}$$

where the calculation of P_{ref} is the same as grid-forming mode, K_{PQ} represents the ratio between active and reactive power, P_{INV} represents the measured active power of the inverter, Q_{ref} represents the reference reactive power, ϑ_{PLL} is calculated through a PLL that tracks the real-time phase angle of phase-a voltage at the connecting point, u_{abc} are the real-time voltage measured at the connecting point, and G_{PLL} is the gain of the PLL. Other parts of the grid-following control loops are the same as grid-forming control loops and will not be repeated here.

2.2.2 Control Strategy of Inverter 2

Inverter 2 is a grid-forming inverter that uses virtual synchronizing generator control. This inverter can operate with the same control parameters in both grid-connected mode and island mode, and can autonomously provide frequency and voltage support in both operating modes. It can take external demand as power reference when operating under the grid-connected mode, and provide exact power for the load when operating under the island mode. This inverter contains three internal control loops: power loop, voltage loop, and current loop, its control configurations are demonstrated in Figure 5.

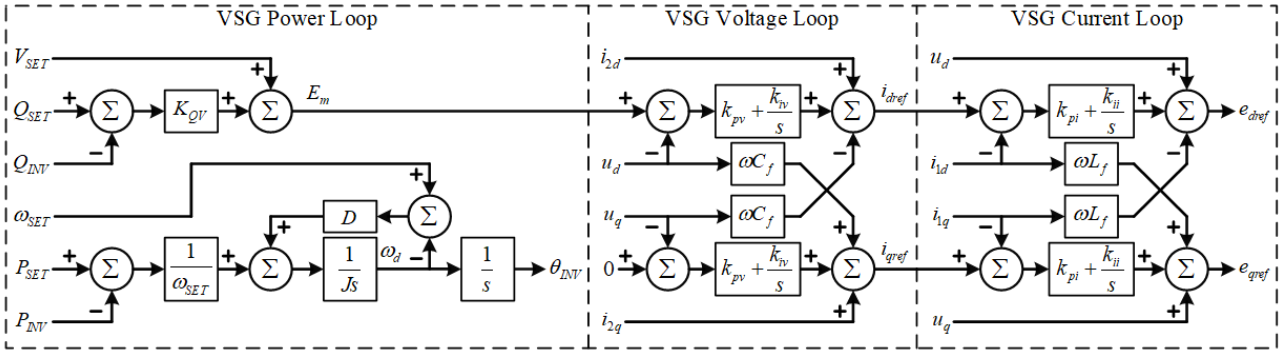

Figure 5 VSG control loops.

Equation (10) demonstrates the power loop using VSG control:

$$\begin{bmatrix}\theta_{INV}\\ E_m\end{bmatrix}=\begin{bmatrix}\dfrac{D\omega_{SET}}{s(Js+D)}+\dfrac{P_{SET}}{s(Js+D)\omega_{SET}}\\ V_{SET}+K_{QV}Q_{SET}\end{bmatrix}-\begin{bmatrix}\dfrac{P_{INV}}{s(Js+D)\omega_{SET}}\\ K_{QV}Q_{INV}\end{bmatrix} \tag{10}$$

where P_{SET} represents the rated active power of the inverter, J represents the inertia coefficient, D represents the damping coefficient, ϑ_{INV} represents the inverter reference phase angle, Q_{SET} represents the rated reactive power of the inverter, Q_{INV} represents the measured reactive power of the inverter, K_{QV} represents the Q-V droop coefficient, and E_m represents the reference voltage.

Equation (11) demonstrates the voltage loop using dq-decoupling control:

$$\begin{bmatrix}i_{dref}\\ i_{qref}\end{bmatrix}=\begin{bmatrix}k_{pv}+\dfrac{k_{iv}}{s} & 0\\ 0 & k_{pv}+\dfrac{k_{iv}}{s}\end{bmatrix}\begin{bmatrix}E_m\\ 0\end{bmatrix}+\begin{bmatrix}i_{2d}\\ i_{2q}\end{bmatrix}+\begin{bmatrix}-\left(k_{pv}+\dfrac{k_{iv}}{s}\right) & -\omega C_f\\ \omega C_f & -\left(k_{pv}+\dfrac{k_{iv}}{s}\right)\end{bmatrix}\begin{bmatrix}u_d\\ u_q\end{bmatrix} \tag{11}$$

where C_f is the LC filter's capacitance, k_{pv} and k_{iv} are the parameters of a PI controller.

Equation (12) demonstrates the current loop using dq-decoupling control:

$$\begin{bmatrix}e_{dref}\\ e_{qref}\end{bmatrix}=\begin{bmatrix}k_{pi}+\dfrac{k_{ii}}{s} & 0\\ 0 & k_{pi}+\dfrac{k_{ii}}{s}\end{bmatrix}\begin{bmatrix}i_{dref}\\ i_{qref}\end{bmatrix}+\begin{bmatrix}-\left(k_{pi}+\dfrac{k_{ii}}{s}\right) & -\omega L_f\\ \omega L_f & -\left(k_{pi}+\dfrac{k_{ii}}{s}\right)\end{bmatrix}\begin{bmatrix}i_{1d}\\ i_{1q}\end{bmatrix}+\begin{bmatrix}u_d\\ u_q\end{bmatrix} \tag{12}$$

where L_f is the LC filter's inductance, k_{pi} and k_{ii} are the parameters of a PI controller.

2.2.3 Configuration of Back-To-Back Converter

The proposed back-to-back converter is a three-terminal device. The AC side of the DC/AC converters at each terminal is connected to one microgrid as shown in Figure 3, and each converter uses PLL to achieve synchronization with its respective microgrid. The DC sides of the three converters share a common capacitor as shown in Figure 6. Both inverters connected with microgrid 1 and microgrid 2 work under grid-following mode and use the control strategy demonstrated in Section 2.2.1. The converter connected with synchronous generator region works as rectifier to transmit active power only. One important thing is that the proposed back-to-back converter will only transmit active power between different microgrid regions, and the reactive power is only provided by the grid-forming inverter or synchronous generator in each microgrids. Therefore, the frequency sensitivity in different microgrids can be different and will not be influenced by other microgrids, and the isolation of the power parameters can be achieved. The circuit structure of the back-to-back converter is demonstrated in Figure 6.

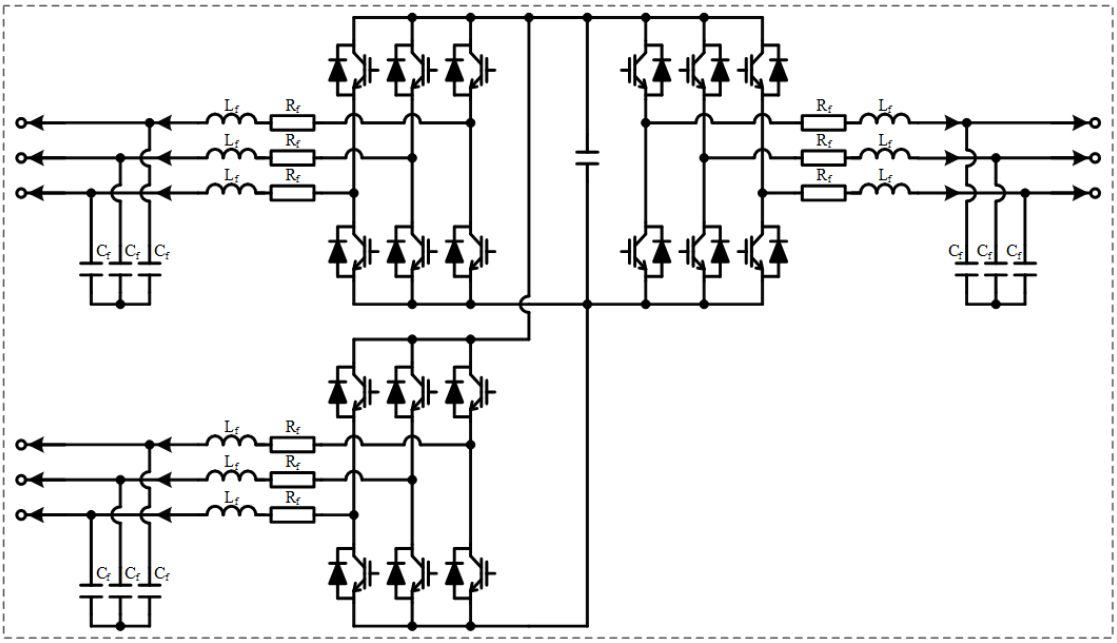

Figure 6 Circuit structure of the back-to-back converter.

The circuit structure at each terminal is the same as the three-phase inverter with an LC filter, and the number of terminals can decrease or increase as much as the number of microgrids. The output active power at each terminal of the back-to-back converter must satisfy the equation presented below to ensure power balance and stable operation.

$$\sum_{i=n} P_i = 0 \tag{13}$$

where P_i represents the output active power of the i^{th} terminal of the back-to-back converter, and n represents the number of terminals of the back-to-back converter. As long as the total sum of each terminal's output power is 0, the power balance in the modified system can be achieved.

3. Simulation Results

Three cases have been conducted in simulations, in each of which the system RoCoF, inverter output power, and inverter DC-side input power are demonstrated and compared when disturbances occur at different locations. In Case 1, the original multimachine system with direct connection is adopted while in Case 2 and Case 3 a modified system with proposed back-to-back converters is used. Power sharing is disabled in Case 2 while a 50% power sharing is enabled in Case 3. All three cases have the same settings below: (1) The overall system is rated to operate at 415 V, 60 kW; (2) Each inverter and synchronous generator has a 20 kW local constant load and a 10 kW switchable load (also named as disturbance); (3) The system reaches steady state at 4.0 s; the first switchable load which is close to inverter 1 is turned on at 5.0 s and lasts for one second, after a short transient, the system recovers to steady state; the second switchable load which is close to inverter 2 is turned on at 8.0 s and lasts for one second, after another short transient, the system recovers to steady state; the third switchable load which is close to synchronous generator is turned on at 11.0 s and lasts for one second.

3.1 Case 1 Direct Connection of Inverters and Synchronous Generator

Case 1 simulates the original multimachine system in which all inverters and synchronous generators are directly connected to one PCC point. The circuit structure for this study is shown in Figure 2. The dynamic performance is demonstrated in Figure 7 and detailed numerical results are listed in Table 1.

Table 1 Numerical results of case 1.

Parameters (min/max)	Steady state	Disturbance 01	Disturbance 02	Disturbance 03
f-PCC (Hz)	49.99/50.01	49.99/50.01	49.92/50.08	49.98/50.02
RoCoF (Hz/s)	-00.15/00.15	-00.18/00.19	-00.94/00.95	-00.43/00.46
P-CF (kW)	20.03/20.13	19.84/29.75	20.05/20.21	20.03/20.17
P-DC-CF (kW)	20.84/21.00	20.65/30.69	20.83/21.02	20.84/20.98
P-STATCOM (kW)	-00.06/00.04	-00.31/00.19	-00.12/00.06	-00.10/00.04
P-VSG (kW)	19.95/20.06	19.90/20.12	10.46/30.04	18.69/21.37
P-DC-VSG (kW)	20.83/20.94	20.78/21.00	11.16/31.21	19.54/22.28
P-SG (kW)	19.97/20.08	19.97/20.12	15.92/34.63	19.91/30.01

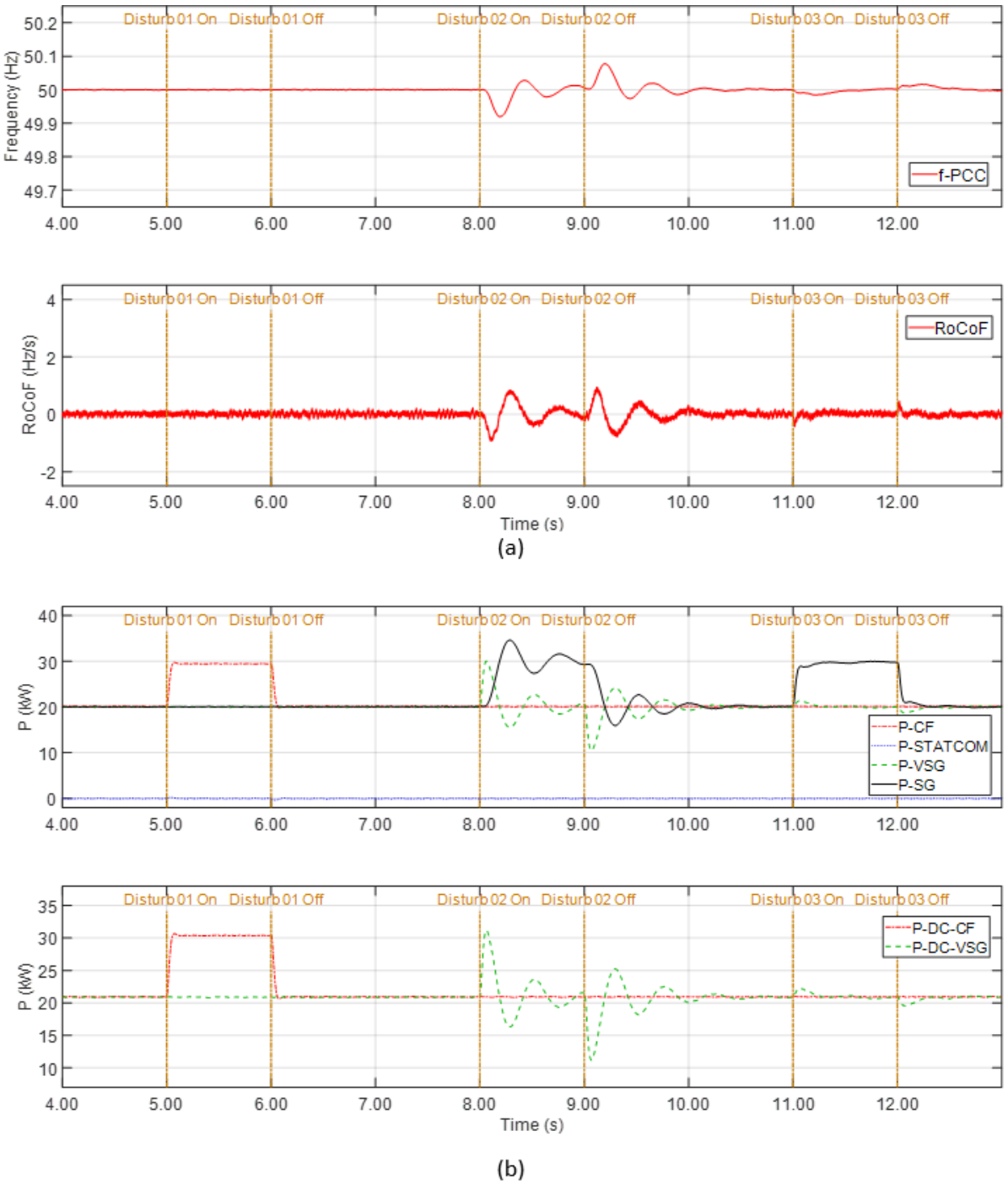

Figure 7 (a) Dynamic frequency and RoCoF of the original multimachine system. (b) Dynamic output power of the original multimachine system.

It can be seen that in case 1, the system has small frequency fluctuations (49.99-50.01 Hz) and small RoCoF (-0.15-0.15 Hz/s) during steady state. When the disturbance close to CF inverter occurs, all additional power is provided by the DC source of CF inverter with 96.9% efficiency, and the frequency fluctuations (49.99-50.01 Hz) and RoCoF (-0.18-0.19 Hz/s) remains low due to the fast response capability of CF inverter. When the disturbance close to VSG inverter occurs, the additional power is simultaneously provided by both the DC source of VSG inverter with 96.3% efficiency and the SG, and the frequency fluctuations (49.92-50.08 Hz) and RoCoF (-0.94-0.95 Hz/s) are large due to the power oscillation between VSG inverter and SG. When the disturbance close to SG occurs,

the additional power is mostly provided by the SG, and the frequency fluctuations (49.98-50.02 Hz) and RoCoF (-0.43-0.46 Hz/s) are mild due to the inertia in SG. The detailed results of each part in case 1 are presented in Table 1.

3.2 Case 2 Microgrids Separation Using a Back-to-Back Converter (0 Power-Sharing)

Case 2 simulates the modified system in which a three-terminal back-to-back converter is placed at the original PCC point to separate the original system into three different microgrids, where each part has its unique grid impedance and still can share power with other parts through the back-to-back converter. In this study, the power-sharing value is set as 0 kW to highlight the dynamic difference only caused by this proposed separation method. The circuit structure of the modified system is shown in Figure 3. The dynamic performance is demonstrated in Figure 8 and detailed numerical results are listed in Table 2.

Table 2 Numerical results of case 2.

Parameters (min/max)	Steady state	Disturbance 01	Disturbance 02	Disturbance 03
f-Microgrid 01 (Hz)	49.99/50.01	49.98/50.03	49.99/50.01	49.99/50.01
RoCoF-01 (Hz/s)	-01.18/01.29	-01.60/02.78	-01.09/01.38	-01.22/01.20
P-CF (kW)	20.02/20.18	19.82/29.73	19.93/20.14	19.96/20.19
P-DC-CF (kW)	20.83/20.96	20.63/30.67	20.74/20.96	20.77/21.03
P-STATCOM (kW)	-00.17/00.04	-00.30/00.24	-00.08/00.02	-00.16/00.03
f-Microgrid 02 (Hz)	49.99/50.00	49.99/50.00	49.73/50.00	49.99/50.00
RoCoF-02 (Hz/s)	-00.36/00.36	-00.39/00.35	-01.95/01.85	-00.32/00.35
P-VSG (kW)	19.94/20.07	19.91/20.10	19.96/30.53	19.98/20.12
P-DC-VSG (kW)	20.82/20.94	20.79/20.98	20.84/31.72	20.86/21.00
f-Microgrid 03 (Hz)	50.00/50.00	50.00/50.00	50.00/50.00	49.98/50.02
RoCoF-03 (Hz/s)	-00.05/00.05	-00.06/00.04	-00.03/00.05	-00.79/00.75
P-SG (kW)	22.06/22.28	22.02/22.30	21.59/22.37	21.65/32.29

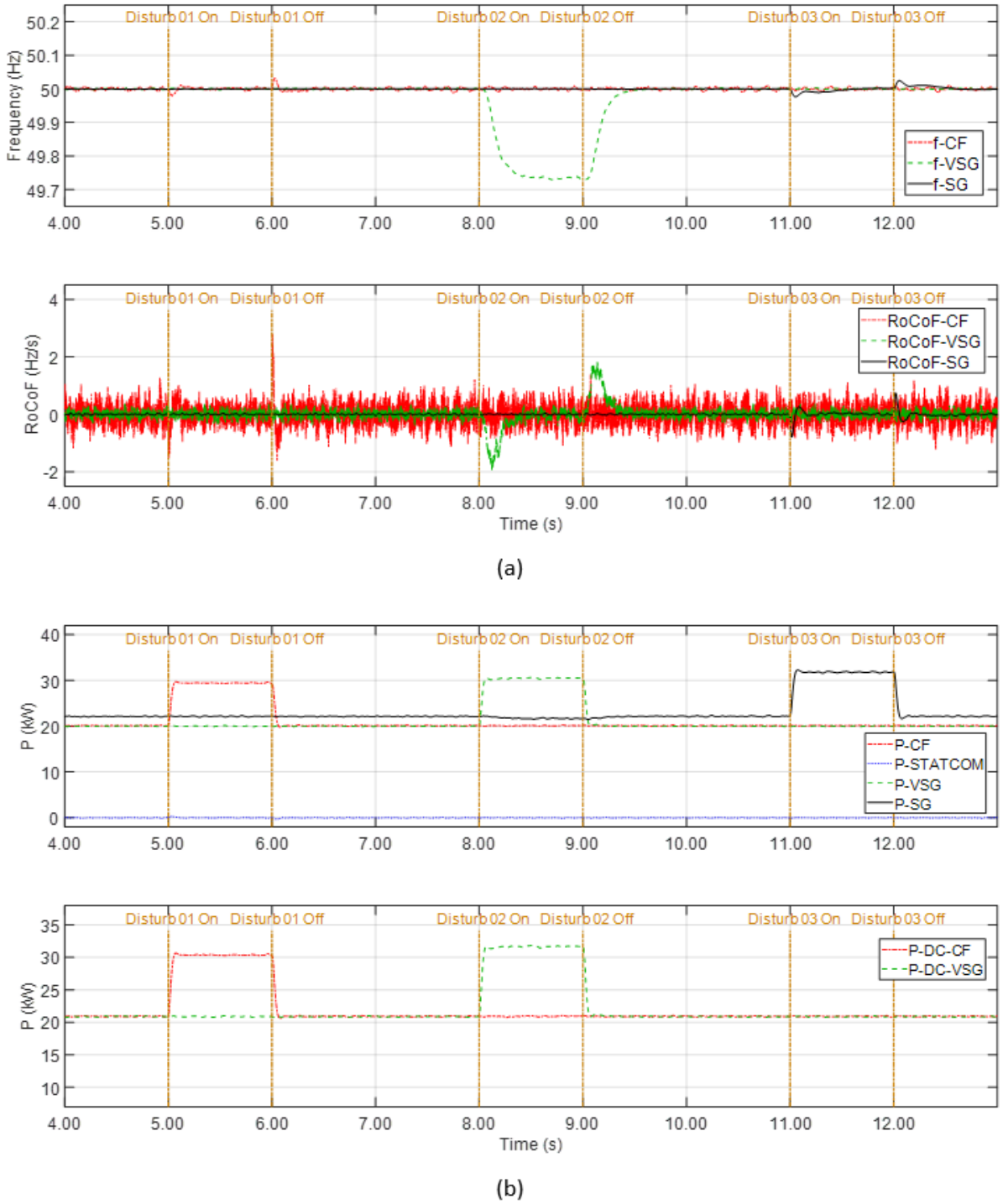

Figure 8 (a) Dynamic frequency and RoCoF of the modified system (0 power-sharing). (b) Dynamic output power of the modified system (0 power-sharing).

It can be seen that in case 2, all three Microgrids separated by back-to-back converter have small frequency fluctuations (Microgrid 01: 49.99-50.01 Hz, Microgrid 02: 49.99-50.00 Hz, Microgrid 03: 50.00-50.00 Hz) and small RoCoF (Microgrid 01: -1.18-1.29 Hz/s, Microgrid 02: -0.36-0.36 Hz/s, Microgrid 03: -0.05-0.05 Hz/s) during steady state. When the disturbance close to CF inverter occurs, all additional power is provided by the DC source of CF inverter with 96.9% efficiency, and the frequency fluctuations (49.98-50.03 Hz) and RoCoF (-1.60-2.78 Hz/s) are mild due to the fast response capability of CF inverter. When the disturbance close to VSG inverter occurs, all additional

power is provided by the DC source of VSG inverter with 96.3% efficiency, and the frequency fluctuations (49.73-50.00 Hz) and RoCoF (-1.95-1.85 Hz/s) are large due to the virtual inertia of VSG inverter. When the disturbance close to SG occurs, all additional power is provided by the SG, and the frequency fluctuations (49.98-50.02 Hz) and RoCoF (-0.79-0.75 Hz/s) are midden due to the inertia in SG. The influence of disturbance is completely isolated through the AC-DC-AC conversion of the proposed back-to-back converter. All power sources in each microgrid operate equivalently under island mode when the power-sharing value is set as 0 kW, and the control over the power characteristics of each microgrid remain isolated with each other. The detailed numerical results of each part in case 2 are presented in Table 2.

3.3 Case 3 Microgrids Separation Using a Back-to-Back Converter (50% Power-Sharing)

Case 3 simulates the modified system with the back-to-back converter. It has the same circuit structure as case 2. The power-sharing value for this case is set as 50% of the disturbances to highlight the dynamic difference caused by power-sharing. One important thing is, in case 3 every 0.5 s before a disturbance occurs, the modified system will be informed of the incoming disturbance value and its location. If the disturbance is located in the microgrid with inverters, then 50% of active power will be transmitted from the microgrid with synchronous generator into the microgrid where the disturbance is going to happen. If the disturbance is located in the microgrid with synchronous generator, other microgrids with inverters will not provide power support, since the synchronous generator is considered as a large power source with huge power capacity and the inverter-based source has limited power redundancy. The dynamic performance of case 3 is demonstrated in Figure 9 and detailed numerical results are listed in Table 3.

Table 3 Numerical results of case 3.

Parameters (min/max)	Steady state	Disturbance 01	Disturbance 02	Disturbance 03
f-Microgrid 01 (Hz)	49.99/50.01	49.98/50.04	49.99/50.01	49.99/50.01
RoCoF-01 (Hz/s)	-01.18/01.04	-01.58/03.34	-01.27/01.21	-01.15/01.20
P-CF (kW)	20.06/20.21	15.22/25.04	20.00/20.31	20.00/20.18
P-DC-CF (kW)	20.87/21.02	16.00/25.90	20.83/21.12	20.81/20.99
P-STATCOM (kW)	-00.09/00.02	-00.49/00.40	-00.10/00.02	-00.13/00.11
f-Microgrid 02 (Hz)	49.99/50.00	49.99/50.00	49.86/50.13	49.99/50.00
RoCoF-02 (Hz/s)	-00.31/00.33	-00.43/00.35	-01.92/01.78	-00.39/00.38
P-VSG (kW)	19.92/20.07	19.85/20.10	14.74/25.36	19.88/20.13
P-DC-VSG (kW)	20.80/20.96	20.73/20.99	15.51/26.42	20.76/21.01
f-Microgrid 03 (Hz)	50.00/50.00	49.99/50.01	49.99/50.01	49.98/50.02
RoCoF-03 (Hz/s)	-00.05/00.05	-00.09/00.09	-00.08/00.08	-00.79/00.78
P-SG (kW)	22.03/22.20	21.77/27.50	21.69/27.66	21.61/32.30

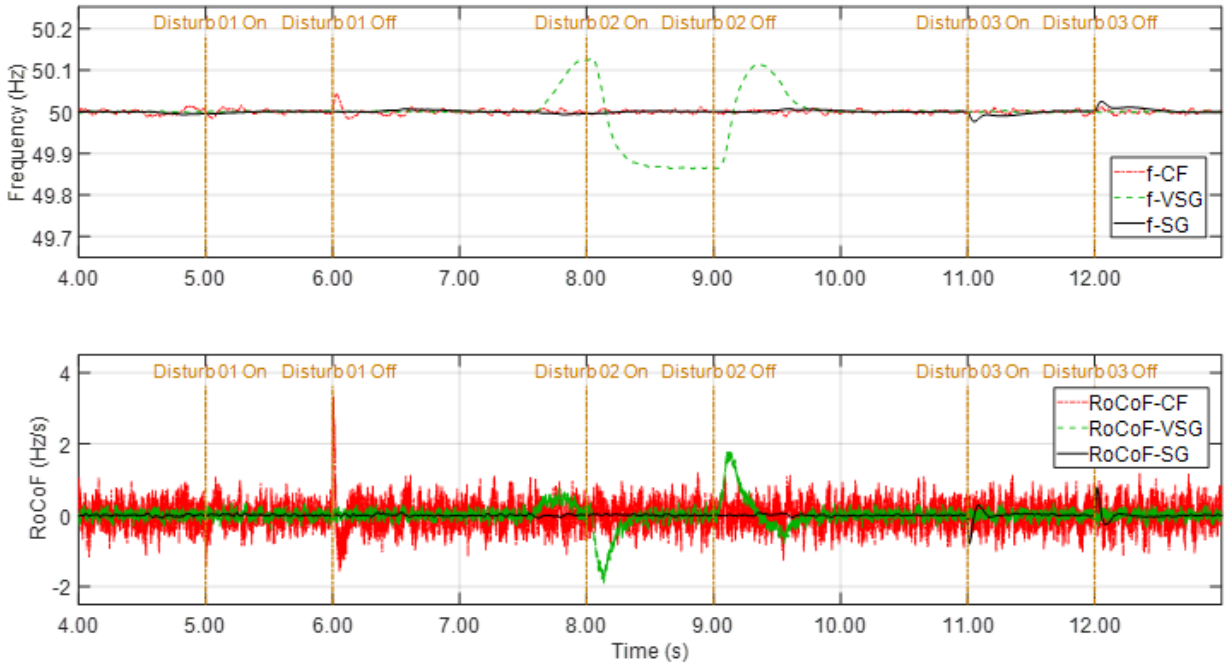

(a)

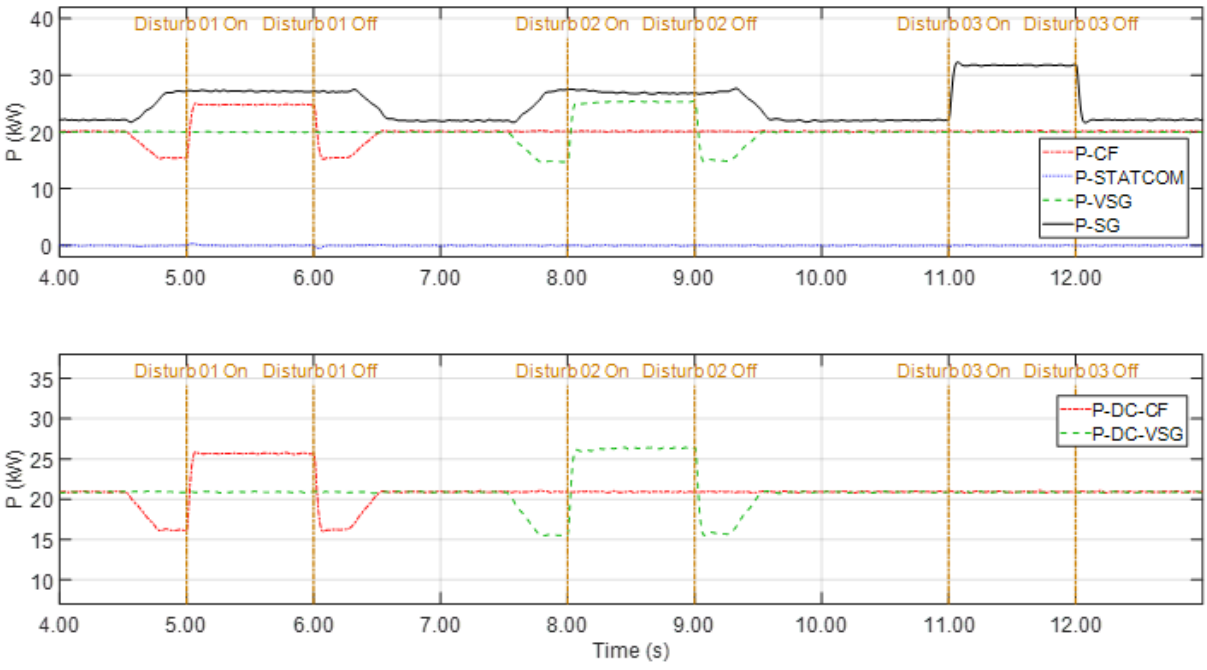

(b)

Figure 9 (a) Dynamic frequency and RoCoF of the modified system (50% power-sharing). (b) Dynamic output power of the modified system (50% power-sharing).

It can be seen that in case 3, all three microgrids separated by back-to-back converter have small frequency fluctuations (Microgrid 01: 49.99-50.01 Hz, Microgrid 02: 49.99-50.00 Hz, Microgrid 03: 50.00-50.00 Hz) and small RoCoF (Microgrid 01: -1.18-1.29 Hz/s, Microgrid 02: -0.36-0.36 Hz/s, Microgrid 03: -0.05-0.05 Hz/s) during steady state. When the disturbance close to CF inverter occurs, 50% additional power is provided by the DC source of CF inverter with 96.1% efficiency, while the

remaining 50% is provided by the power transmitted from the microgrid with the SG through the proposed back-to-back converter. The frequency fluctuations (49.98-50.04 Hz) and RoCoF (-1.58-3.34 Hz/s) are mild due to the fast response capability of CF inverter. 50% additional power is provided by the DC source of VSG inverter with 96.0% efficiency, while the remaining 50% is provided by the power transmitted from the microgrid with the SG through the proposed back-to-back converter. The frequency fluctuations (49.86-50.13 Hz) and RoCoF (-1.92-1.78 Hz/s) are large due to the virtual inertia of VSG inverter. When the disturbance close to SG occurs, all additional power is provided by the SG. The frequency fluctuations (49.98-50.02 Hz) and RoCoF (-0.79-0.78 Hz/s) are mild due to the inertia in SG. The influence of disturbance is completely isolated through the AC-DC-AC conversion of the proposed back-to-back converter, and the output power of inverter's DC source has reduced during disturbance due to the additional power shared from SG, and the power characteristics of each microgrids remain isolated with each other. The detailed numerical results of each part in case 3 are presented in Table 3.

4. Discussion

Based on the simulation results of the above cases, it can be seen that the constant frequency inverter performs well when it is the only power source that provides power in the microgrid. However, power oscillation will occur if there are other grid-forming inverters or synchronous generator directly connected to its PCC point. It has smaller frequency fluctuations than the VSG inverter during steady state, but larger frequency deviations when encountering disturbances. The control method of the constant frequency inverter needs to be further improved. The proposed grid separation method using a three-terminal back-to-back converter successfully separates the original multimachine system into three microgrids with two being the inverters-based regions while the other being synchronous generator-based region, thereby reducing power oscillation between the grid-forming inverters and synchronous generator at steady state while keeping the capability to transmit power between different microgrids.

When external communication equipment, such as remote terminal units (RTU), fiber optic communication units, modems and routers, provides detailed information about the incoming disturbance before it occurs, e.g. a factory informing the power grid on the expected additional power it might take before it turns on the machines, the proposed back-to-back converter can proactively draw additional power from the region with synchronous generators which has higher power generation capacity and transmit it to the inverter-based microgrid where the factory is located. The overall output power from the DC source of inverter can be reduced. Figure 10 demonstrates the comparison of the inverter's DC source output power between the original multimachine system with direct connection and the modified system using the proposed back-to-back converter with 50% power-sharing capability. It can be seen that when encountering same 10 kW disturbance, the maximum DC power of CF inverter is reduced from 30.67 kW to 25.90 kW, and the maximum DC power of VSG inverter is reduced from 30.53 kW to 25.36 kW. This means that the battery storage for these inverter-based microgrid can be significantly reduced while maintaining the same dynamic performance when encountering disturbances.

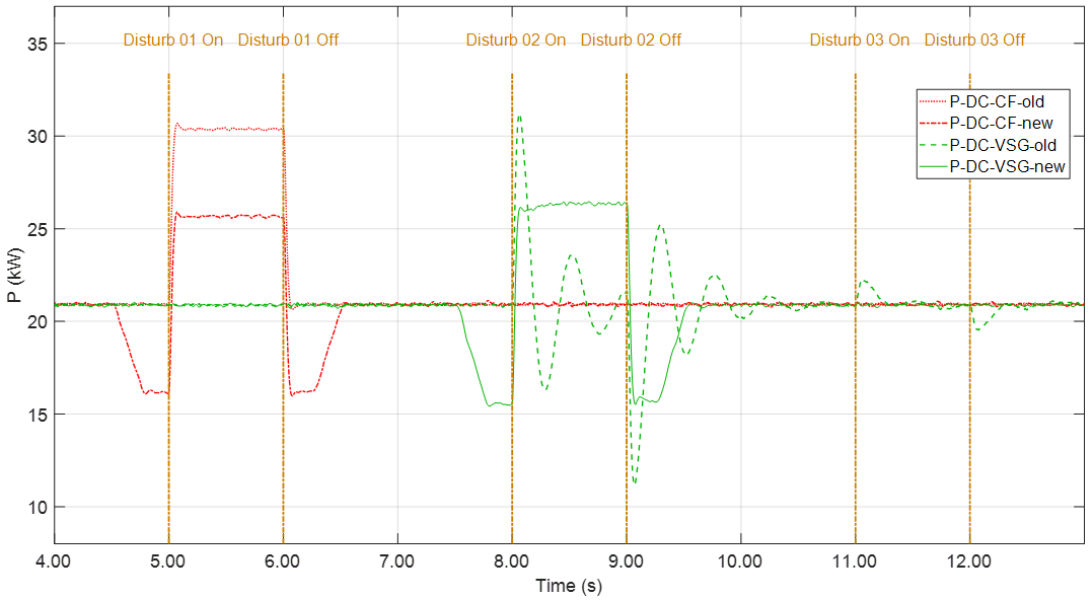

Figure 10 Inverter DC power comparison between original and modified system.

Compared with the existing direct connection method, the advantages and disadvantages of this proposed grid-separation method with back-to-back converter are presented below:

Advantages:

- Complete isolation of different power sources in large grid
- Reduce power oscillation between different power sources
- Accurate control of output power at each power sources during disturbance
- Reduce battery storage requirement of inverter-based power sources

Disadvantages:

- Extra cost for this back-to-back equipment
  (this cost can continue to reduce with the development of power electronic technique)
- Requirement of additional communication equipment
  (communication equipment is very important for distributed system)

5. Conclusions

This paper proposed a grid separation method using a multi-terminal back-to-back converter. It is designed to be placed at the PCC point of the original multi-machine system and can separate the original multimachine system into multiple microgrid regions while keeping the capability to share power between different microgrids. Each of the two inverter-based microgrids has one grid-forming inverter and another grid-following inverter which is part of the back-to-back converter and unique grid impedance. While the third microgrid region contains a synchronous generator and another rectifier which is part of the back-to-back converter and unique grid impedance. The synchronous generator-based microgrid is used to transmit additional power to other inverter-based microgrids when encountering more power demand in their regions. The simulation of the original multimachine system that has two inverters, one STATCOM, one synchronous generator, and three constant loads is conducted to examine the stability. Both inverters being grid-forming inverters, one using constant frequency control and the other using VSG control. For such an operation, there is a power oscillation between the grid-forming inverters and synchronous

generator. In contrast, this oscillation or instability problem has been significantly reduced in the modified system with the back-to-back converter since the operating condition for the grid-forming inverters has changed from grid-connected mode into the island mode due to the separation by the back-to-back converter. When there is external communication or prediction method that can provide detailed information about the incoming load demand before it takes place, the proposed back-to-back converter can transmit additional power from the synchronous generator-based region into the inverter-based microgrids, reducing the requirement for battery storage while maintaining the same dynamic performance.

Abbreviations

SG	Synchronous Generator
PCC	Point of Common Coupling
STATCOM	Static Synchronous Compensator
GFL	Grid Following
GFM	Grid Forming
PLL	Phase-Locked Loop
SMIB	Single-Machine-Infinite-Bus
VSG	Virtual Synchronous Generator
FRT	Fault Ride-Through
SCR	Short Circuit Ratio
RTU	Remote Terminal Unit

Acknowledgments

This journal paper is inspired by the collaboration work of Minyang Wang and Daming Zhang. The authors acknowledge Dr Sara Ashfaq's contribution in the discretized modeling of synchronous generators.

Author Contributions

The first author proposed the separation method and did all the research work of this study. The second author developed the constant frequency control used in this study. The third author helped with the background used in this study.

Funding

We express our genuine gratitude for the support provided by the Chinese Scholarship Council (CSC), CSC NO. 202208200017.

Competing Interests

The authors have declared that no competing interests exist.

References

1. Chow JH. Enabling inverter-based resource stability control in power systems with high renewable penetration. CSEE J Power Energy Syst. 2023; 9: 1248-1250.
2. Sarkar BD, Gupta L, Shankar R. Modeling adoption of sustainable green energy: An integrated approach using FERA. IEEE Trans Eng Manag. 2024; 71: 5907-5920.
3. Xia W, Wang Z, Wang J, Guo J, Wang K, Han P. Evaluation of minimum safety inertia of new energy power system considering rate of change of frequency. Proceedings of the 2022 12th International Conference on Power and Energy Systems (ICPES); 2022 December 23-25; Guangzhou, China. Piscataway, NJ: IEEE.
4. Guo X, Yuan X, Zhu D, Zou X, Hu J. Evaluation and optimization of DFIG-based WTs for constant inertia as synchronous generators. IEEE Trans Power Electron. 2024; 39: 10453-10464.
5. Mohammed N, Zhou W, Bahrani B. Comparison of PLL-based and PLL-less control strategies for grid-following inverters considering time and frequency domain analysis. IEEE Access. 2022; 10: 80518-80538.
6. Zhou W, Mohammed N, Bahrani B. Comprehensive modeling, analysis, and comparison of state-space and admittance models of PLL-based grid-following inverters considering different outer control modes. IEEE Access. 2022; 10: 30109-30146.
7. Yuan H, Qin X, Li W, Su L, Shen G, Xin H. Small signal stability analysis of grid-following inverter-based resources in weak grids with SVGs based on grid strength assessment. Proceedings of the 2021 IEEE 1st International Power Electronics and Application Symposium (PEAS); 2021 November 13-15; Shanghai, China. Piscataway, NJ: IEEE.
8. Kumar N, Wagh P, Kolhe D, Arane P, Kadlag P. Power quality improvement in distributed energy resources for EV charging using STATCOM. Proceedings of the 2022 1st International Conference on Sustainable Technology for Power and Energy Systems (STPES); 2022 July 04-06; SRINAGAR, India. Piscataway, NJ: IEEE.
9. Kumar R, Diwania S, Khetrapal P, Singh S. Performance assessment of the two metaheuristic techniques and their hybrid for power system stability enhancement with PV-STATCOM. Neural Comput Appl. 2021; 34: 3723-3744.
10. Wang M, Meng K, Yuan L, Liang Z. Comparative synthetic inertia assessment between droop and virtual synchronous generator control for weak grids integration. Proceedings of the 2022 IEEE 5th International Electrical and Energy Conference (CIEEC); 2022 May 27-29; Nanjing, China. Piscataway, NJ: IEEE.
11. Fu S, Sun Y, Li L, Liu Z, Han H, Su M. Power oscillation suppression of multi-VSG grid via decentralized mutual damping control. IEEE Trans Ind Electron. 2022; 69: 10202-10214.
12. Yuan L, Meng K, Huang J, Dong ZY. Investigating subsynchronous oscillations caused by interactions between PMSG-based wind farms and weak AC systems. Int J Electr Power Energy Syst. 2020; 115: 105477.
13. Wang M, Meng K, Yu L, Yuan L, Liang Z. Comparative fault ride through assessment between grid-following and grid-forming control for weak grids integration. Proceedings of the 2022 IEEE Global Conference on Computing, Power and Communication Technologies (GlobConPT); 2022 September 23-25; Delhi, India. Piscataway, NJ: IEEE.
14. Wang M, Zhang Y, Ahmed AD, Meng K. Dynamic response of grid-following and grid-forming inverters when encountering disturbances. Proceedings of the 2023 IEEE International

Conference on Energy Technologies for Future Grids (ETFG); 2023 December 03-06; Wollongong, Australia. Piscataway, NJ: IEEE.

15. Zhang D. Modeling of autonomous microgrid operated at medium-voltage level and at constant frequency and study of its voltage profile. J Energy Power Technol. 2023; 5: 009.
16. Zhang D. Issues on autonomous ac microgrid operated at constant frequency. Proceedings of the 2021 31st Australasian Universities Power Engineering Conference (AUPEC); 2021 September 26-30; Perth, Australia. Piscataway, NJ: IEEE.